Striated AKR Emission: A Remote Tracer of Ion Solitary Structures

R.L. Mutel,[1] J .D. Menietti,[1] I. W. Christopher,[1] D. A. Gurnett,[1] J. M. Cook[1]

Abstract.
We describe the statistical properties of narrowband drifting auroral kilometric radiation ('striated' AKR) based on observations from the Cluster wideband receiver during 2002-2005. We show that the observed characteristics, including frequency drift rate and direction, narrow bandwidth, observed intensity, and beaming angular sizes are all consistent with triggering by upward traveling ion solitary structures ('ion holes'). We calculate the expected perturbation of a horseshoe electron distribution function by an ion hole by integrating the resonance condition for a cyclotron maser instability (CMI) using the perturbed velocity distribution. We find that the CMI growth rate can be strongly enhanced as the horseshoe velocity distribution contracts inside the passing ion hole, resulting in a power gain increase greater than 100 dB. The gain curve is sharply peaked just above the R-mode cut-off frequency, with an effective bandwidth ≤50 Hz, consistent with the observed bandwidth of striated AKR emission. Ion holes are observed *in situ* in the acceleration region moving upward with spatial scales and speeds consistent with the observed bandwidth and slopes of SAKR bursts. Hence, we suggest that SAKR bursts are a remote sensor of ion holes and can be used to determine the frequency of occurrence, locations in the acceleration region, and lifetimes of these structures.

1. Introduction

Auroral kilometric radiation (AKR) bursts exhibit a wide variety of fine structure as seen on frequency-time spectra. The cyclotron maser instability (CMI) [*Wu and Lee*, 1979] is widely assumed to be the basic plasma mechanism responsible for the emission. This mechanism originally assumed a loss-cone electron velocity distribution function, but in situ observations in the acceleration region have shown that a 'horseshoe' or crescent distribution is more accurate [*Louarn et al.*, 1990; *Roux et al.*, 1993; *DeLory et al.*, 1998; *Ergun et al.*, 2000]. The horseshoe distribution, which arises naturally for electron beams in the presence of inhomogeneous magnetic fields [*Speirs et al.*, 2005], provides a robust and efficient free energy source for the CMI mechanism, as shown both by model calculations [e.g. *Pritchett*, 1984; *Pritchett et al.*, 1999; *Bingham and Cairns*, 2000] and in laboratory experiments [e.g., *Speirs et al.*, 2005]. This mechanism has been applied not only to terrestrial AKR emission, but to many astrophysical environments in which the requisite conditions (low density, beamed electrons, inhomogeneous magnetic fields) are thought to be present, e.g. planetary magnetospheres [*Zarka*, 1998; *Farrell et al.*, 2004], stellar magnetospheres [*Louarn, Le Quéau, and Roux*, 1986; *Kellett et al.*, 2002; *Willes and Wu*, 2004], and even relativistic jets in active galaxies [*Begelman et al.*, 2005].

Detailed physical models for the rich variety of observed spectral signatures are still an active area of research. AKR fine structure exhibits many morphologies on time-frequency spectra, including slowing drifting or nearly stationary features lasting tens of seconds [*Gurnett et al.*, 1979], drifting features which may be interacting with each other [*Pottelette et al.*, 2001], and periodically modulated or banded

emission [*Grabbe*, 1982]. Although some AKR bursts appear to be broadband emission extending over 100's of kilohertz [*Hanasz et al.*, 2001], the total power is dominated by highly time-variable fine structures, especially during periods of enhanced bursts [*Morozova et al.*, 2002], suggesting that perhaps all AKR radiation is a superposition of narrowband, short duration fine structures.

Gurnett et al. [1979] first suggested that drifting AKR fine structure may be due to localized sources rising and falling along auroral magnetic field lines, with emitted frequency equal to the local electron cyclotron frequency. *Gurnett and Anderson* [1981] suggested that the emission is triggered by electrostatic waves which drift along the field at the local ion-acoustic speed. An early detailed model which attempts to explain AKR fine structure is the tuned cavity model of *Calvert* [1982] in which the source region acts as a waveguide with sharp density boundaries. The source emits radiation in normal modes analogous to an optical laser, resulting in narrowband emission which drifts as the wave packet propagates into regions of varying width. A related idea is that of *Farrell* [1995] in which the cavity boundary is oscillating quasi-periodically. Under these conditions, broadband radio photons will be stochastically accelerated, resulting in quasi-monochromatic discrete tones, whose frequencies slowly drift with changes in the cavity geometry. A difficulty with these models is that they require special conditions (e.g. sharp density boundaries, oscillating walls) which are not supported by observations [*Pritchett et al.*, 2002].

Several authors have reproduced AKR fine structure using electromagnetic particle simulations to model the AKR source region. *McKeen and Winglee* [1991] used a one-dimensional electromagnetic particle-in-cell (PIC) code to model the cyclotron maser instability in a plasma with an inhomogeneous magnetic field. They found that radiation is emitted in individual packets which combine to form drifting features that both rise and fall, consistent with some types of AKR fine structure. Both X- and O-mode drifting fine structures are created, consistent with observations [*Benson et al.*, 1988] but not predicted in feedback models such as *Calvert* [1982]. A weakness of their model is that predicted drift rates are generally much higher than observed drifts.

---

[1]Dept. Physics and Astronomy, University of Iowa, Iowa City IA 52242, USA.
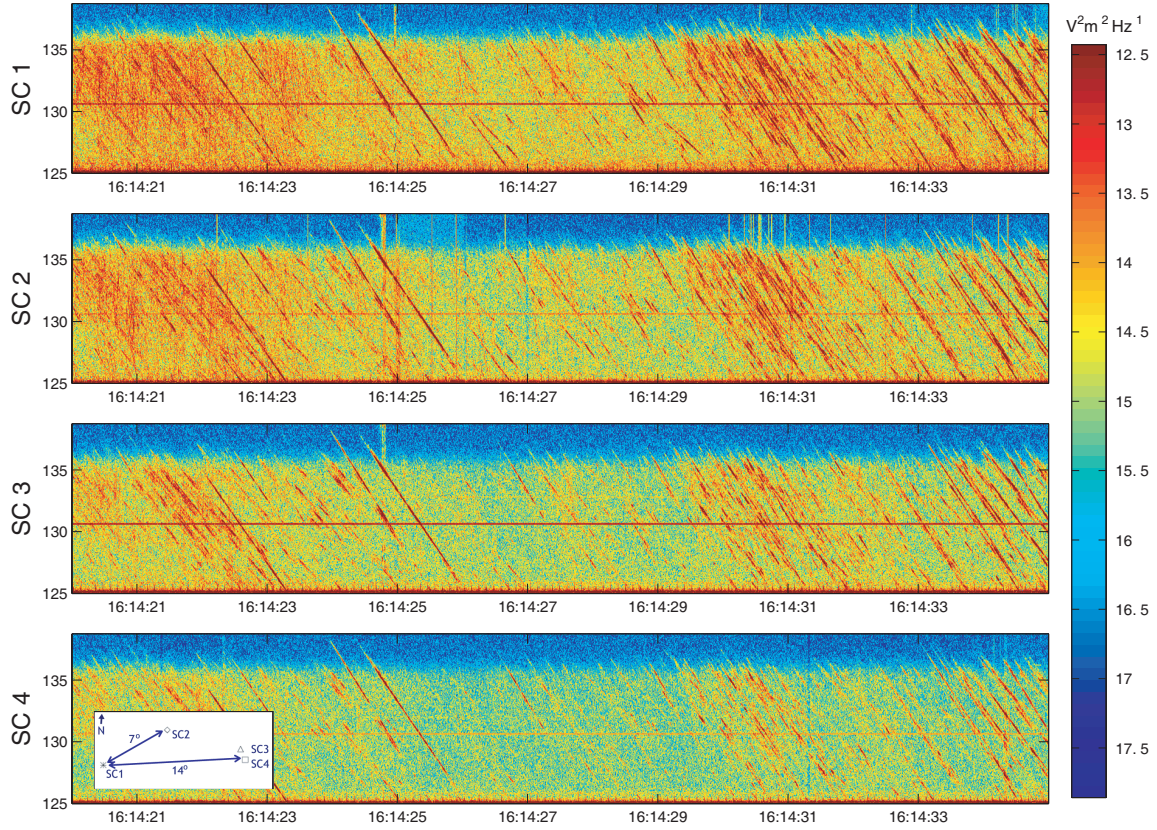
Figure 1. Frequency-time spectra of striated AKR bursts observed on 4 Cluster spacecraft on August 31, 2002 from 16:14:20 - 16:14:35 UT. The inset shows the projected angular separations of the spacecraft as seen from the source.

Pritchett et al. [2002] used a 2-dimensional PIC code with model parameters based on in situ FAST spacecraft measurements of the AKR source region. The simulated AKR is most strongly amplified longitudinally and consists entirely of short-timescale fine structures. The predicted bandwidth ($\Delta\omega/\omega \sim 10^{-3}$) is somewhat larger than at least some observed AKR fine structure.

More recently, Pottelette and colleagues have investigated the possible connection between AKR fine structure and electron holes [*Pottelette et al.*, 2001, 2003] and also tri-polar structures [*Pottelette and Treumann*, 2005]. AKR radiation from small packets ('elementary radiation sources') associated with the holes are thought to be strongly amplified as the packets slow down and are reflected from the field-aligned electric field. Since the scale size of electron holes is very small (a few Debye lengths, *Bounds et al.* [1999]), the observed narrow bandwidth of AKR fine structures is easily accounted for. However, since neither the observed speeds or direction of electron holes (1000 - 2500 km s^{-1} always downward, [*Bounds et al.*, 1999]) are representative of fine structure frequency drifts, there is not a straightforward relationship between the observed properties of electron holes and the dynamics of the AKR fine structure.

In this paper, we present evidence that a particular type of AKR fine structure called striped or striated AKR [*Menietti et al.*, 1996, 2000] is triggered by ion solitary structures (ion holes). In section 2 we present new observations of SAKR bursts, including new bandwidth and angular beamwidth measurements. In section 3 we calculate the change in CMI gain for a density depleted region with a pre-existing horseshoe velocity distribution when perturbed by a passing ion hole. We compare the observed proper-

ties of SAKR with those calculated by radiation generated from the CMI instability in an ion hole. In section 4 we discuss some inferred properties of ion holes, such as lifetimes, probability of occurrence as a function of location, and radial dependence of speed, that cannot be inferred from single spacecraft in situ measurements.
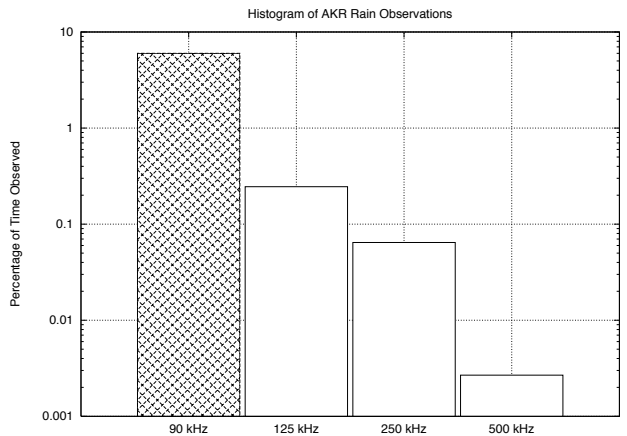
Figure 2. Frequency of occurrence of SAKR as a function of observing frequency. The data for 90 kHz (hatched bar) is from *Menietti et al.* [2000].

2. Observed properties of SAKR

Striated AKR (SAKR) consists of trains of narrowband drifting bursts with negative slopes in the range -2 to -20 kHz s^{-1}, corresponding to upward-traveling sources with speeds between 100 - 1,000 kms^{-1}. Figure 1 shows a typical dynamical spectrum of SAKR bursts observed with the Cluster wideband (WBD) plasma wave instrument [*Gurnett et al.*, 1997] on the four Cluster spacecraft. The bursts were observed in the 125-135 kHz band between 16:14:20 - 16:14:35 UT on 31 August 2002. Although the spectra are similar on all four spacecraft, there are clear differences in individual striations, indicative of angular beaming on the scale of the projected spacecraft separations, as shown in the inset at lower left. Also, individual bursts have very narrow bandwidths and are nearly always observed in groups with spacing between bursts of 30-300 ms. These characteristics are described in more detail below.

2.1. Occurrence frequency

The occurrence probability of SAKR emission is quite low at frequencies above 100 kHz: We detect SAKR bursts in less than 1% of all WBD spectra observed when the spacecraft was above 30°magnetic latitude (Note that below this latitude, there is often shadowing by the Earth's plasmasphere.) The occurrence probabilities were computed by dividing the number of dynamic spectra (length 52 sec) for which SAKR emission was clearly detected by the total number of spectra over a one year interval (July 2002 to 2003). This overestimates the actual occurrence probability for SAKR since we do not correct for the fractional time within each spectrum that SAKR is present.

There is a strong inverse correlation with observing frequency as shown Figure 2. There are only few detections in several hundred hours of data in the 500-510 kHz band (detection probability $p < 0.01\%$), while $p \sim 0.2\%$ in the 125-125 kHz band. *Menietti et al.* [1996, 2000] also studied SAKR emission using the plasma wave instrument (PWI) receiver on the Polar spacecraft. They also found an inverse correlation with observing frequency, with a 6% detection rate in the 90 kHz band (Fig. 2, shaded bar) and comparable probabilities and overlapping frequencies. By contrast, non-striated AKR emission is frequently detected, especially during sub-storm onset. The occurrence probability of AKR is nearly 30% for geomagnetic index K_p in the range $1 < K_p < 3$, with the highest occurrence frequency in the winter polar regions [*Kumamoto et al.*, 1998].

2.2. Frequency drift and speed

SAKR bursts have negatively sloped, nearly linear morphologies, at least within the normally sampled bandwidth (9.5 kHz) of the WBD receivers. The majority of the slopes range between -2 kHz s^{-1} and -8 kHz s^{-1}. Assuming the emission frequency is identified with the local electron gyrofrequency, the speed of the stimulator as a function of frequency and slope can be written

$$V = 540 \text{km s}^{-1} \cdot \left(\frac{\alpha}{10\,\text{kHz}\,\text{s}^{-1}}\right)\left(\frac{100\,\text{kHz}}{f}\right)^{\frac{4}{3}} \quad (1)$$

where V is the stimulator speed (kms^{-1}), α is the observed slope of the SAKR burst (kHz s^{-1}), f is the observed frequency (kHz), and we have assumed the source moves upward along a dipolar magnetic field line at magnetic latitude $\lambda_M = 70°$. Figure 3 shows a histogram of the observed slopes of 650 SAKR burst events observed in the 125-135 kHz band along with the derived trigger speeds (top x axis). The mean slope is -5.6 kHz s^{-1}, with more than 90% of the slopes in the range -2 to -8 kHz s^{-1}. The corresponding trigger speeds, using equation 1, are in the range 76 – 303

km s^{-1}, with a mean value 213 km s^{-1}. These results are similar to those reported by *Menietti et al.* [2000].

Figure 5 shows a group of SAKR bursts detected on one spacecraft while operating the WBD instrument in a wider bandwidth (77 kHz) mode. Over this wider bandwidth, the striations are not linear, but rather have a curved, frequency-dependent slope. The curve can be fit by assuming a source radiating at the local electron cyclotron frequency and moving with constant speed along a field line in a dipolar magnetic field. The overlaid white line shows the expected trace for a source moving upward at a constant velocity of 300 kms^{-1}. SAKR bursts with similar frequency-dependent behavior are seen in Plate 1 of [*Menietti et al.*, 2000].

The altitude range of the SAKR locations are shown on the right y-axis. For this example, individual bursts originated near 6500 km altitude and moved upward at 300 kms^{-1} to an altitude near 8100 km, implying a lifetime of several seconds. We have examined several other SAKR events with wide bandwidth and have found that all exhibit similar lifetimes and have nearly constant speed, although the speed varies with epoch.
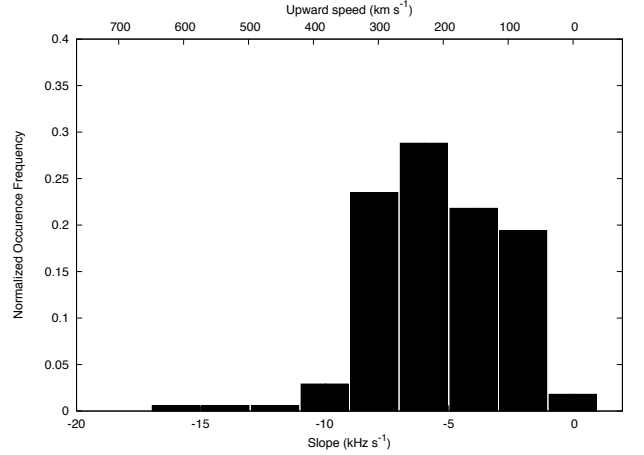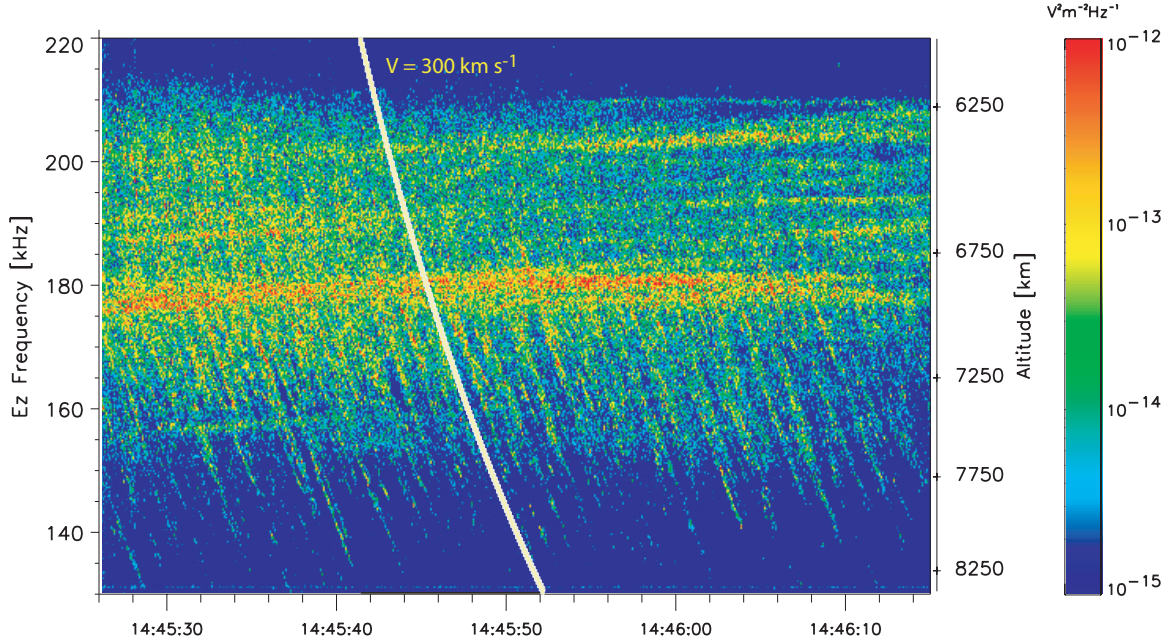

Figure 3. Histogram of observed SAKR burst slopes in the 125-135 kHz band (bottom x-axis) and derived trigger speed (top x-axis, from equation 1).
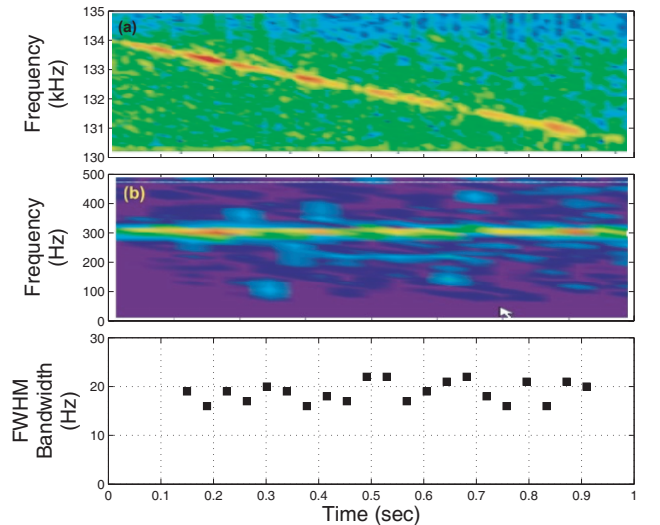
Figure 4. SAKR bandwidth. (a) SAKR burst observed with Cluster WBD, (b) Same burst, but detrended, (c) Measured bandwidth in 37 ms intervals.

Figure 5. Striated AKR bursts observed on Cluster spacecraft SC2 on Jan 15, 2005 from 14:45:26 to 14:46:15 UT. Individual burst trails extend from 180 kHz to 135 kHz, corresponding to an altitude range from 7,000 km to 8,100 km. The yellow line is a calculated trail for a constant velocity source moving upward at 300 km s^{-1}. Note that the SAKR bursts appear to originate at or near an intense, slowly drifting AKR source at $\sim$ 7000 km.

2.3. Coeval broadband AKR emission

SAKR bursts are almost always detected superposed on broader band AKR emission. This can be clearly seen in both Figure 1 and 5, as well as in Plate 1 of *Menietti et al.* [2000]. This appears to be a universal characteristic of SAKR, except in cases where the SAKR intensity is so low that underlying broadband emission may have been undetected. Background AKR emission coeval with SAKR bursts is consistent with the hypothesis that ion holes trigger the SAKR bursts (section 3.2) since the CMI gain in the source region is significant even in the absence of the ion holes.

2.4. Bandwidth

One of the most unusual features of SAKR bursts is their extraordinarily narrow bandwidth. The top panel of Figure 4 shows a single isolated SAKR burst. The middle panel shows the same feature, but after de-trending by subtraction of a 'chirp' signal of best-fit constant negative slope. The lower panel shows the full width at half maximum of a Gaussian fit along the frequency axis of the de-trended signal after summing in time intervals of 37 ms each. The resulting bandwidths, in the range 15 – 22 Hz, are much narrower than previously reported either observationally (e.g. *Gurnett et al.* 1979) or resulting from model calculation of AKR emission (e.g. *Pritchett et al.* 1999; *Yoon and Weatherwax* 1998) although *Baumback and Calvert* [1987] also reported AKR bandwidths as small as 5 Hz. (In the latter paper, the bursts do not appear to be SAKR emission). Other SAKR bursts we have examined have bandwidths ranging from 15 to 40 Hz.

The narrow bandwidth implies a small source extent along the z (B-field) direction, viz,

$$\Delta z = 0.55 \, km \cdot \left[\frac{100 \, kHz}{f} \right]^{\frac{4}{3}} \left[\frac{\Delta f}{10 Hz} \right] \qquad (2)$$

where Δz is the source extent along the B field and Δf is the observed bandwidth. For $f = 130$ kHz and $\Delta f = 20$ Hz we obtain $\Delta z = 0.76$ km. This is considerably smaller

than the lateral extent of the AKR source region and indicates the trigger for SAKR must have a dimension along the magnetic field of order 1 km.

2.5. Angular Beam Size

The Cluster spacecraft array has the unique ability to simultaneously sample the flux density of individual AKR bursts at four widely separated points in space. By comparing the flux density on pairs of spacecraft, we can estimate the average angular beam size of individual bursts. The beaming probability is defined using the following algorithm. For each pair of spacecraft during a given observation, we calculate the projected angular separation between spacecraft as seen from a location situated above the magnetic pole of the hemisphere being observed, at a height corresponding to the electron cyclotron frequency at the center frequency of each observing band (e.g., 2.35 R$_e$ for the 125-135 kHz band). This constitutes an average AKR location in that band without regard to location on the auroral oval. We next correct for differential propagation delay by shifting the waveform data from each spacecraft to the distance of the nearest spacecraft. We then divide the time-frequency spectrum from each spacecraft pair (52 sec duration for 125-135 kHz band) into data 'cells' 19 msec x 53 Hz in size. This window was chosen to match the observed bandwidth of SAKR (cf. section 2.4) but the beaming results are not very sensitive to the data window size. We computed the angular beam size with data windows factors of two smaller and larger, and the results did not differ significantly.

The intensities are normalized to correct for differing distances between individual spacecraft and the AKR source. We then omit from further analysis all data cells whose intensities are below a threshold, arbitrarily chosen to be 10 dB below the maximum flux density for that spectrum. Finally, we compare intensities in each pair of data windows, assigning a weight 1 to pairs for which the intensities are within 10 dB of each other, and 0 otherwise. The overall beaming probability for each angular separation interval is the sum of the beaming weights divided by all cell pairs.

Note that this scheme is susceptible to overestimation of the beaming probability, since it is possible that independent AKR sources will illuminate separate spacecraft at the same frequency and time interval. This 'confusion' problem is smaller for SAKR emission since it is often clear from the burst morphology on a time-frequency spectrum that only one source contributes to a given data cell at one time, whereas with normal AKR there are very often several intersecting sources which contribute to a given data cell.

In Figure 6 we plot the beaming probability versus angular separation for 651 SAKR bursts in the 125-135 kHz and 250-260 kHz bands. We have fitted a Gaussian function to the 125 kHz band observations using a least-squares fitting algorithm. The resulting full width at half maximum (FWHM) angular size is $\theta = 5.0°$ (solid angle $\Omega = 0.006$ sr). This is surprisingly small compared with most previously published observations of AKR beam size (e.g. *Green and Gallagher* [1985]), who reported beaming solid angles of 4.6 sr and 3.3 sr at 178 and 100 KHz respectively. They made angular beaming estimates by comparing time-averaged spectra observed using two satellites (Hawkeye and IMP-6) which simultaneously observed AKR bursts while the spacecraft were both over the same polar region. Since the time resolution used for the Hawkeye-IMP6 spectrum comparison (several minutes) far exceeds the time-scale of individual AKR bursts, their measured angular beam is actually a measure of the ensemble-averaged sky distribution of AKR bursts over a several minute time-scale rather than the angular beam size of individual AKR emission sources. This is the confusion problem mentioned above.

An important unanswered question is the 2-dimensional structure of the SAKR burst angular beam pattern: It is asymmetric, or perhaps a hollow cone as suggested by *Calvert* [1987]? Since the spatial frequency coverage of the Cluster spacecraft array is often nearly one-dimensional at high magnetic latitude, it is difficult to analyze the 2-dimensional structure of individual bursts. The angular beaming probability plot shown in Figure 6 includes measurements over a range of baseline orientations. However, a preliminary analysis of beaming probability grouped by baseline orientation did not reveal any obvious trends. We are presently analyzing a much a larger dataset consisting of a large variety of AKR emission and wider range of baseline orientations to investigate the 2-dimensional structure of the AKR angular beam.

2.6. Individual SAKR Source Power Estimate

The angular beaming observations, combined with measured flux density, allow a direct estimate of the average intrinsic power of individual SAKR bursts. For intense SAKR bursts, the observed square of the electric field intensity is

$$I_\nu \sim (1-10) \times 10^{-12} \text{ (V/m)}^2 \text{ Hz}^{-1} \qquad (3)$$

at a source-spacecraft distance $d = 10\text{R}_e$. Converting to flux density, we obtain

$$S_\nu = I_\nu/Z_0 \sim (0.3-3) \times 10^{-14} \text{ W m}^{-2} \text{ Hz}^{-1} \qquad (4)$$

where $Z_0 = 377$ ohms is the impedance of free space. This flux density range is about one hundred times smaller than the flux density of intense AKR bursts reported by *Benson and Fainberg* [1991]. This is consistent with the conjecture that intense AKR bursts are the sum of many spatially distinct 'elementary radiation sources' [*Pottelette et al.*, 2001]

The power emitted at the AKR source is the isotropic power corrected by the angular beamsize of an individual SAKR burst

$$P = 4\pi d^2 \cdot S_\nu \cdot \Delta\nu \cdot \frac{\Omega}{4\pi} \qquad (5)$$

where $\Delta\nu \sim$ 20-50 Hz is the bandwidth of a burst, and $\Omega \sim 0.006$ sr, is the solid angle of the emission beam. Using these values, the resulting power is P $\sim$ 1 – 10 W, much smaller than the previous estimates of P $\sim 10^3$-10^4 W for a single 'elementary radiator' [*Pottelette et al.*, 2001].

3. Connection with ion holes

Ion solitary structures, also known as ion holes, are small-scale ($\sim$1km) regions of negative electrostatic potential associated with upgoing ion beams. They are seen in spacecraft electric field measurements as symmetric bipolar parallel electric field structures with amplitudes 10 – 500 mV m^{-1} and timescales 3-10 ms. They were first detected in S3-3 spacecraft observations [*Temerin et al.*, 1982] and have been subsequently been studied using in situ measurements in the acceleration region by several authors (e.g. *Bounds et al.* [1999]; *Dombeck et al.* [2001]; *McFadden et al.* [2003]). Ion holes travel upward at speeds between 75-300 kms^{-1} [*Bounds et al.*, 1999; *Dombeck et al.*, 2001] (although *McFadden et al.* [2003] argue for somewhat higher speeds, in the range 550 - 1100 kms^{-1}). The width of the waves increase with amplitude [*Dombeck et al.*, 2001] which is inconsistent with small amplitude 1-d soliton models, but which supports a BGK-type generation mode [*Muschietti et al.*, 2002].

3.1. Electron distribution function and CMI growth rate

AKR radiation arises from wave growth resulting from the interaction of a radiation field with an electron velocity distribution having a positive slope in the direction perpendicular to the magnetic field ($\partial f/\partial \text{v}_\perp > 0$). The condition for waves of angular frequency ω and wave normal angle θ to resonate with electrons with angular frequency ω_{ce} and velocity v is given by [*Wu and Lee*, 1979]

$$k_\parallel v\cos\theta - \omega + n\frac{\omega_{ce}}{\gamma\left(v_\parallel, v_\perp\right)} = 0 \qquad (6)$$
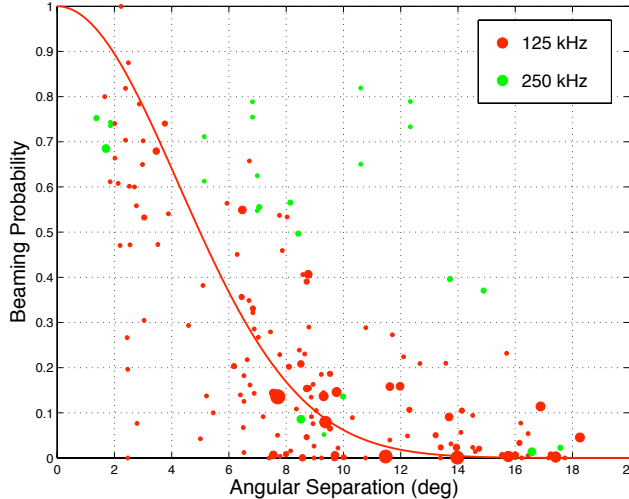

Figure 6. Angular beamsize for 651 individual SAKR burst sources measured at 125 kHz (red dots) and 250 kHz (green dots) using observed correlations between multiple spacecraft. The size of each point is proportional the number of bursts for that point. The fitted FWHM beamsize is 5.0°.

where ω_{ce} is the electron cyclotron frequency, n is an integer, and γ is the Lorentz factor of the relativistic electrons. The cyclotron maser instability (CMI) is the case $n=1$. If we assume that the electrons are mildly relativistic, as is observed in the AKR source region ($E_e \sim 10$ keV, so $\gamma \sim 1.01$), we can expand the Lorentz factor to obtain the equation for a circle in velocity space
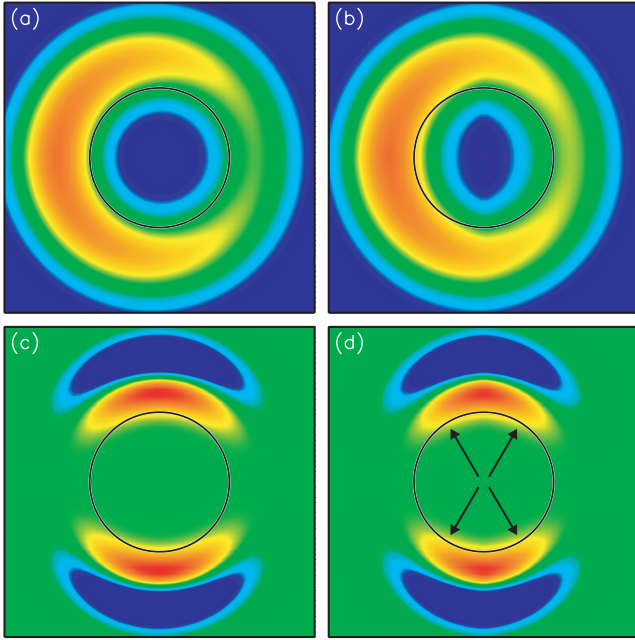
$$v_\perp^2 + \left(v_\parallel - v_c\right)^2 = v_r^2 \qquad (7)$$

where the resonant circle's center is on the horizontal axis displaced by

$$v_c = \frac{k_\parallel}{\omega_{ce}} c^2 \qquad (8)$$
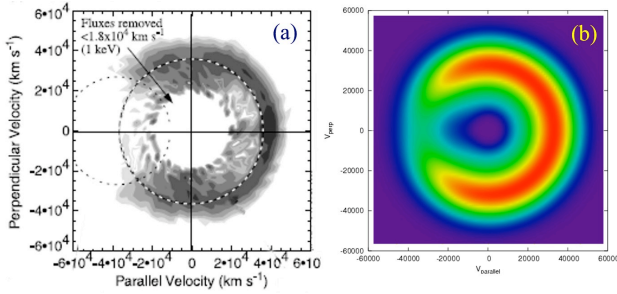
Figure 7. (a) Electron distribution function measured by FAST in AKR source region [*Ergun et al.*, 2000]. (b) Model distribution.

Figure 8. Top panel: horseshoe electron velocity distribution function outside an ion hole (a), and inside an ion hole (b). Black circle is the CMI resonant circle. The $v_\parallel$ direction is the horizontal axis, Earthward to left. Bottom panel: weighted partial derivative $\partial f/\partial v_\perp$ outside an ion hole (c), and inside an ion hole (d). The arrows indicate the parts of the growth line integral (equation 9) enhanced inside the hole.

and the radius of the resonant circle is

$$v_r = v_c \left[1 - \frac{2c^2\left(\omega - \omega_{ce}\right)}{v_c{}^2 \omega_{ce}}\right]^{\frac{1}{2}} \qquad (9)$$

Analysis of recent FAST observations of AKR emission in the source region [*Ergun et al.*, 1998, 2000; *Pritchett et al.*, 1999] provides evidence, based on wave polarization, that the AKR k-vector direction at the source is nearly perpendicular to the B field ($k_\parallel \sim 0$). The E-field of the wave is polarized perpendicular to the ambient magnetic field which indicates that the wave is purely X-mode [*Strangeway et al.*, 2001]. In the following, we explicitly assume $k_\parallel = 0$, so that the radius of the resonance circle becomes

$$v_r = c \left(\frac{-2\delta\omega}{\omega_{ce}}\right)^{\frac{1}{2}} \qquad (10)$$

where $\delta\omega = \omega - \omega_{ce}$. The growth rate of the CMI mechanism is given by calculating the imaginary part of the angular frequency,

$$\omega_i = \frac{\pi^2 \omega_{pe}^2}{4\omega n_e} \oint v_\perp^2 \frac{\partial f}{\partial v_\perp} dv_\perp \qquad (11)$$

where the $v_\perp$ integral is performed on the closed circular path given by equation 4.

The electron velocity distribution in the upward current acceleration region has been measured *in situ* by both Viking [*Roux et al.*, 1993] and FAST [*DeLory et al.*, 1998]
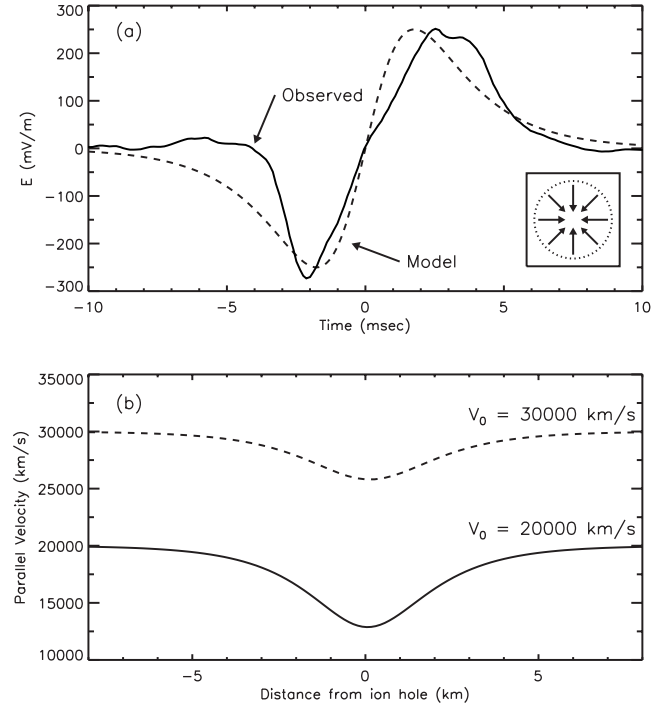
Figure 9. (a) Observed electric field vs. time (solid line) as an ion hole passes by FAST spacecraft [*McFadden et al.*, 2003], and best-fit model (dashed line) using equation (14). The inset at lower right shows a simple spherical model of an ion hole with inward electric field. (b) Calculated parallel velocity vs. distance from an ion hole for an electron passing through an ion hole with an impact parameter 1 km and initial velocities 20,000 km s^{-1} (dotted line) and 30,000 kms^{-1} (solid line). The assumed hole speed is 300 kms^{-1}.
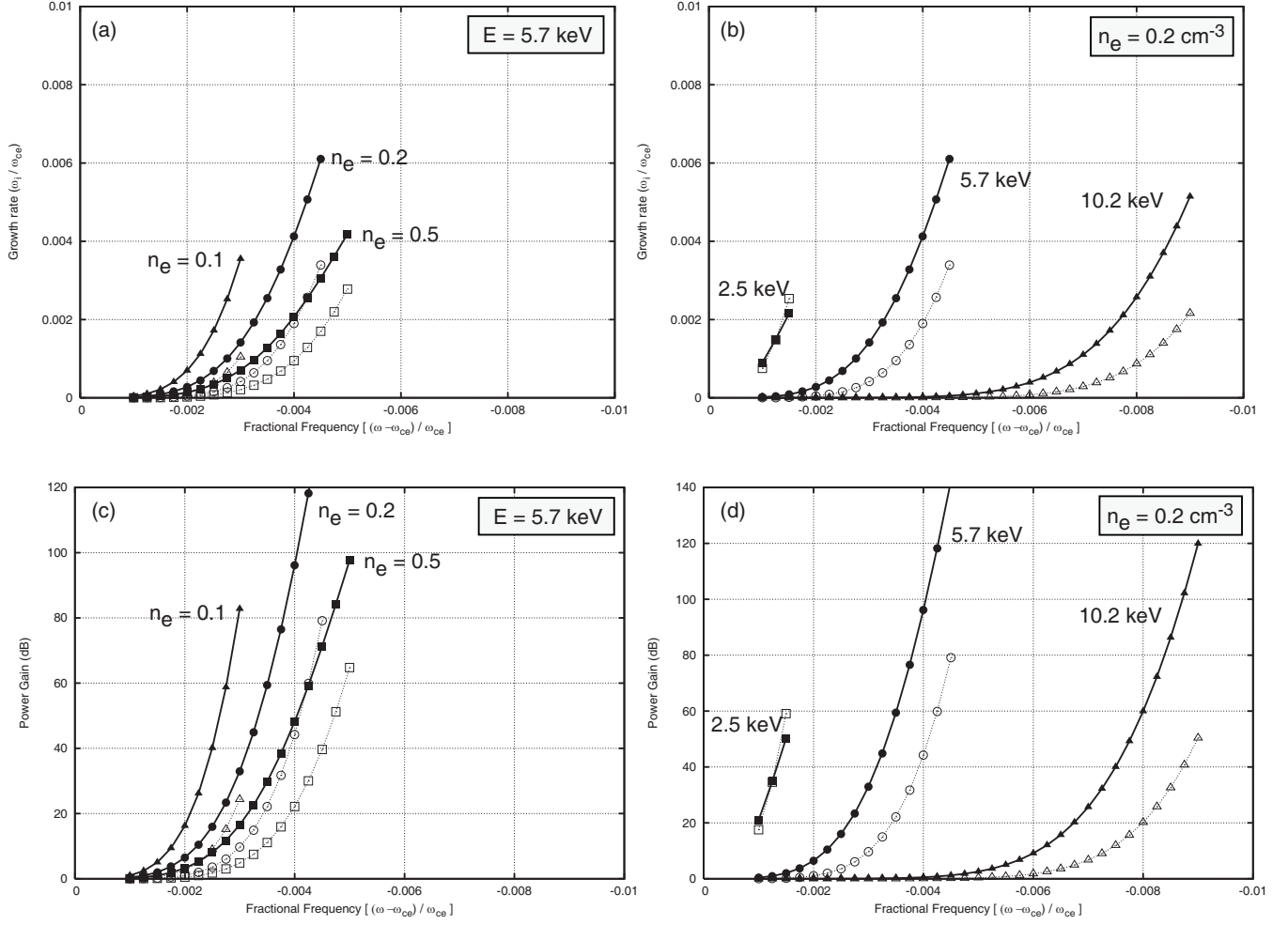
Figure 10. (a) Temporal growth rate as a function of fractional frequency for electron horseshoe distribution radius $V_c/c = 0.15$ ($\bar{E} = 5.7$ keV) and electron density $n_e = 0.1$ cm^{-3}($\triangle$), 0.2 cm^{-3} ($\square$), and 0.5 cm^{-3} ($\circ$). Solid lines are inside ion hole; dashed lines are outside ion hole. (b). Same as (a), but with fixed $n_e = 0.2$ cm^{-3} and $V_c/c = 0.10$ (2.5 keV,$\square$), 0.15 (5.7 keV,$\circ$), 0.20 (10.2 keV, $\triangle$). (c) CMI power gain vs. fractional frequency, same parameters as (a). (d) CMI power gain vs. fractional frequency, same parameters as (c).

spacecraft. It consists of an incomplete shell or 'horseshoe' shape in velocity space. The density of cold electrons (E $\ll 1$ keV) in this region is much smaller than the hot electron population which comprises the horseshoe component [*Strangeway et al.*, 1998]. In this paper we assume that all electrons are in the hot component.

We have modeled the observed velocity distribution using a simple analytic functional form

$$f(v) = g(v) \exp\left[-\left(\frac{v - v_0}{\Delta} \right)^2 \right] \qquad (12)$$

where Δ is the horseshoe width, v_0 the horseshoe radius and the loss-cone function $g(v)$

$$g(v) = 1 - \beta \cdot \text{sech}\left(\frac{\tan^{-1}(v_y/v_x)}{\Theta} \right) \qquad (13)$$

where β is a dimensionless scaling factor and Θ is the characteristic opening angle of the loss cone. The model velocity distribution function is shown in Figure 7 along with a mea-

sured velocity distribution function from FAST [*Ergun et al.*, 2000].

3.2. Triggering SAKR emission by an ion hole

The range of possible interactions between background electrons and ion holes is very complex and varied [*Eliasson and Shukla*, 2005]. These include trapping of electrons between ion holes, excitation and trapping of high-frequency Langmuir waves from electron streams resulting from ion hole collisions, and modification of the ion holes via the ponderomotive force. In this paper we will tacitly assume that the ion holes are well-spaced and non-interacting, and that the only significant effect on the electron population is a transient speed decrease as the electrons traverse the hole's negative potential well. This assumption is motivated by the relatively simple structure of SAKR bursts and by the success in using this assumption to explain all significant observed properties of SAKR bursts. Other more complicated forms of AKR fine structure seen on dynamical spectra may well involve one or more of the complex interactions mentioned above.

Since the electrons are magnetized (gyro-radius r$_{ce}$ $\sim$50m, much smaller than the ion hole parallel scale size r$_{ISS}$ $\sim$1 km), the ion's hole's effect on the perpendicular velocity

component is negligible (a small **ExB** drift, $V_D \sim 40$ m s^{-1}). However, the parallel velocity component will experience a significant decrease as the electrons are repelled by the negative potential well of the hole. To determine the magnitude of the effect, we have modeled the observed electric field structure of an ion hole using the analytic form

$$E(t) = E_0 \tanh\left(\frac{t}{\tau}\right) \text{sech}\left(\frac{t}{\tau}\right) \quad (14)$$

Figure 9a shows an observed E-field of an ion hole along with a plot of the model E-field with $E_0 = 500$ mV m^{-1}, and $\tau = 2$ ms.

We used this model to calculate the velocities of electrons as they traverse the hole for a variety of impact parameters and initial speeds. For initial parallel speeds of 20,000 and 30,000 kms^{-1}, the speed of an electron traversing an ion hole at a minimum distance of 1 km from the center is shown in Figure 9b. As expected, the parallel velocity briefly decreases, so that the horseshoe velocity distribution is 'squeezed' on the parallel (horizontal) axis, as shown in Figure 8b. The speed decrease is proportional to v^{-1} as expected by a simple energy conservation argument: For an electric field E and ion hole diameter L_{ih}, the potential well of the hole is approximately $\Phi \sim E \cdot L_{ih}$. The electron loses kinetic energy as it traverses the potential well, so that energy conservation requires

$$\delta\left(\frac{1}{2}mv_\parallel^2 + q_e\Phi\right) = 0 \quad (15)$$

Solving for the velocity change,

$$\delta v_\parallel = \frac{q_e\Phi}{m_e v_0} \quad (16)$$

For an ion hole electric field E ~ 300 mV m^{-1}, diameter $L_{CMI} \sim 2$km, and $v_0 = 20,000$ kms^{-1}, the expected speed decrease is $\delta v_\parallel \sim 5,000$ kms^{-1}, in good agreement with the exact calculation.

In order to calculate the power gain in the perturbed region, we need an estimate of the convective growth length

$$L_c = \frac{V_g}{|\omega_i|} \quad (17)$$

where V_g is the group velocity of the wave and ω_i is the growth rate. The group velocity is very sensitive to the ratio of plasma to gyro-frequency and the detailed velocity distribution function. As a first approximation, we have used the cold plasma dispersion relations to estimate the group velocity $V_g = d\omega/dk$ for frequencies near the R-mode cut-off frequency. We find that Vg is of order 300 - 1000 km s^{-1}, similar to the estimate used by *Omidi and Gurnett* [1982].

For a maximum growth rate $\omega_i \sim 5000$ s^{-1} (at $\omega_{ce} = 2\pi \times 125$ kHz), the corresponding convective growth length is $L_c \sim 200$m. Hence, there are approximately 5-10 e-folding lengths in the region of the ISS, assuming a perpendicular physical scale of order 1-2 km. This results in a maximum power gain of $e^{10-20} \sim 43$-87 dB. The power gain required to amplify the background radiation to observed levels of normal (wideband) AKR was estimated by *Omidi and Gurnett* [1982] to be e^{20}, which is at the high end of our calculation. However, as discussed above, since SAKR emission is highly beamed, the required power is a factor of ~ 100 smaller, so the requisite power gain is closer to $e^{15} = 65$ dB. This is comfortably within the range predicted by an ion hole trigger.

Figure 10 illustrates the growth rate and power gain both inside and exterior to an ion hole for a range of relativistic electron energies and plasma densities. Figure $10(a, c)$ show the growth rate and power gain respectively for a horseshoe

velocity distribution with a radius $V/c = 0.15$ (E = 5.7 keV) and $n_e = 0.1$, 0.2 and 0.5 cm^{-3}, while Figure $10(b, d)$ shows the growth rate and gain for $n_e = 0.2$ cm^{-3} and a range of radii $V/c = 0.10$, 0.15, and 0.20 (E = 2.5, 5.7, 10.2 keV). These values are typical of the values of electron density and energy observed in the auroral density cavity [*Strangeway et al.*, 1998]. There are several noteworthy features of these plots:

1. The range of electron densities which result in substantial CMI gain is very limited. The maximum density is constrained by the condition that the R-mode cutoff frequency is less than the electron cyclotron frequency. This can by expressed by the inequality

$$\frac{f_{pe}(n_e)}{f_{ce}} < \left[\frac{\gamma - 1}{\gamma}\right]^{1/2} \quad (18)$$

where f_{pe} and f_{ce} are the electron plasma and cyclotron frequencies respectively, and γ is the Lorentz factor. This inequality can also be written

$$n_e < \left(\frac{f_{ce}}{9\text{kHz}}\right)^2 \left(\frac{E}{2E_0}\right) \text{ cm}^{-3} \quad (19)$$

where E_0 is the rest-mass energy of the electron (511 keV). For example, for $E = 5$ keV and $f = 125$ kHz, we find $n_e < 0.9$ cm^{-3}. On the other hand, for very low densities ($n_e << 0.1$ cm^{-3}), the CMI gain decreases dramatically (cf. Fig. $10a$).

2. The gain is a sharply peaked function of frequency. For example, for $n_e = 0.3$ cm^{-3}, $E = 5.7$ keV (Fig. $10c$), a dynamic range of 30 dB near the peak (approximately that observed on dynamic spectra of SAKR bursts) corresponds to a fractional bandwidth $\delta f/f \sim 0.0005$, or $\delta f \sim 50$ Hz at $f = 125$ kHz, in good agreement with observed bandwidths (section 2.4). These extremely narrow bandwidths are characteristic of CMI gain curves with partial-ring velocity distributions [*Yoon and Weatherwax*, 1998].

3. Even outside the ion hole there is substantial CMI gain under some favorable conditions (e.g. 80 dB for the middle plot of Figure $10d$). This may be the explanation for the background AKR seen in Figure 5 and discussed in section 2.3.

3.3. Conversion efficiency

Given the rather small volume of an ion hole, it is reasonable to ask if there is sufficient free energy available from the resonant electrons to power the observed SAKR emission. As shown in section 2.5, the observed flux levels and angular beamwidths of SAKR emission correspond to radiated powers $P_{rad} \sim 1 - 10$ W. Using a an ion hole scale size $L_{ih} \sim 1$ km and speed $V_{ih} \sim 300$ km s^{-1}, and mean electron density and energy $n_e = 0.5$ cm^{-3}, $E_e = 5$ keV respectively, the ratio of radiated power to the electron kinetic energy traversing a hole per unit time is

$$\frac{P_{rad}}{P_{tot}} = \frac{(1-10)W}{n_e E_e L_{ih}^2 V_{ih}} \sim 0.002 - 0.02 \quad (20)$$

This range of conversion efficiencies is similar to previous models of AKR emission [e.g., *Pritchett et al.*, 1999] and indicates that while a single ion hole extracts relatively little energy from the ambient electron population, a train of hundreds of holes traversing the same region could account for a significant modification of the electron distribution function.

4. Discussion

If SAKR bursts are stimulated by upward traveling ion holes in the acceleration region of the magnetosphere, then

observations of these bursts provides a new technique to study characteristics of ion holes such as lifetimes and relative number and speed as a function of altitude, that are impossible to measure with single *in situ* spacecraft .

1. The 77 kHz bandwidth observations of SAKR bursts indicate that ion holes propagate upward for more than 1,000 km, implying lifetimes of a few seconds. This is much longer than estimates of solitary wave lifetimes derived from PIC simulations of solitary waves generated by the two-stream instability [*Crumley et al.*, 2001], which have lifetimes $\tau \sim (100 - 1500)\ \omega_{pe}^{-1} \sim 5$ - 75 ms.

2. The majority of ion hole speeds derived from SAKR observations are in the range 75 - 400 km s^{-1} (Fig. 3). These speeds are in very good agreement with *in situ* measurements of ion hole speeds from Polar (75 - 300 km s^{-1}) at altitudes between 5500 and 7000 km [*Bounds et al.*, 1999; *Dombeck et al.*, 2001]. However, *McFadden et al.* [2003] finds somewhat higher ion hole speeds (550-1100 km s^{-1}) based on data from the FAST satellite at altitudes between 3000 km - 4000 km. It is possible that at speeds above $V \sim 600$ km s^{-1} (slopes >20 kHz s^{-1}) SAKR bursts, especially in closely spaced groups, would be undetected since they would merge into quasi-continuous emission on dynamic spectra.

3. Fits to SAKR bursts assuming a constant speed source, (Fig. 5) indicate that ion holes propagate at nearly constant speed for their entire lifetime. Some numerical simulations [*Crumley et al.*, 2001] show a significant change in ion hole speed as they evolve. This is not supported by our observations.

4. SAKR bursts, and hence ion holes, are much more common at higher altitude, being more than one hundred times as common at 10,000 km ($f_{ce} \sim 90$ kHz) than at 3,200 km ($f_{ce} \sim 500$ kHz) altitude, assuming ambient conditions favorable to the generation of SAKR are not dissimilar in this altitude range.

5. Since SAKR bursts are almost always detected in groups with typical spacing 30 - 300 ms., (section 2.6), this likely also applies to ion holes. Both laboratory plasma experiments [*Frank et al.*, 2001] and observations of ion holes in the magnetosphere [e.g., *Bounds et al.*, 1999] show trains of ion holes with spacings similar to the SAKR bursts.

6. Finally, the uniformity of SAKR intensity and bandwidth over a large frequency range (Fig.5) implies that there is little evolution of the electric field intensity or spatial structure of ion holes over their lifetime.

5. Summary and Conclusions

This paper summarizes the observed properties of a distinct form of auroral kilometric radiation called striated AKR, first described by *Menietti et al.* [1996]. We present new observational results using the WBD instrument on Cluster which characterize the bandwidth and angular beamsize of individual SAKR sources, as well as derived properties such as intrinsic power and speed along the magnetic field.

Assuming the frequency of SAKR bursts can be identified with the local electron cyclotron frequency, the speed and direction of SAKR sources calculated from their observed drift rates are very similar to those observed for ion solitary structures (ion holes) in the upward current region of the magnetosphere. Hence, we investigated whether SAKR bursts could be the result of enhancement of the cyclotron maser instability by ion holes. Using observed electric field signatures of ion holes in this region, we calculate the perturbation caused by the passage of an ion hole on a 'horse-shoe' electron velocity distribution in a dilute ($n_e \ll 1$ cm^{-3}) plasma. The cyclotron maser instability is strongly enhanced inside the ion hole, with power gain exceeding 100 dB in a narrow frequency range just above the x-mode cut-off frequency. These characteristics are in excellent agreement with the observed bandwidth, speed, direction, and flux density of SAKR bursts. Alternative suggestions involving other types of solitary structures to explain AKR fine structure, such as electron holes [*Pottelette et al.*, 2001] or tri-polar structures [*Pottelette and Treumann*, 2005], are not consistent with SAKR properties, although they may be important in other types of AKR fine structures.

If SAKR bursts are in fact triggered by ion holes, a number of derived properties of ion holes can be deduced which would be difficult or impossible to obtain using *in situ* measurements. These include average lifetimes (a few seconds), evolution of propagation speed (nearly constant over lifetime of hole), and relative numbers versus location (much more common high in the acceleration region than near the base).

References

Baumback, M. and Calvert, W., The Minimum Bandwidths of AKR, *Geophys. Res. Lett.*, Vol. 14, 119-122, 1987.

Begelman, M, R. Ergun, and M. Rees, Cyclotron maser emission from blazer jets? *Astrophys. J.*, 625:51-59, 2005.

Benson, R. F. and J. Fainberg, Auroral The maximum power of auroral kilometric radiation *J. Geophys. Res.*, 96,A8, 13749-13762, 1991.

Benson, R., M. Mellott, R. Huff, and D. Gurnett, Ordinary mode auroral kilometric radiation fine structure observed by DE 1, *J. Geophys. Res.*, Vol. 93, xx, 7715-xx, 1988.

Bingham, R. and R. Cairns, Generation of auroral kilometric radiation by electron horseshoe distributions, *Phys. Plasmas*, Vol. 7, 7, 3089-3092, 2000.

Bounds S. R., et al. Solitary Structures Associated with Ion and Electron Beams near 1 Re Altitude, *J. Geophys. Res.*, vol. 104, A12, 28709-28717, 1999.

Calvert, W., A feedback model for the source of auroral kilometric radiation, *J. Geophys. Res..*, 87, 8199, 1982.

Calvert, W., Hollowness of the observed auroral kilometric radiation pattern, *J. Geophys. Res..*, 92, A2, 1267-1270, 1987.

Crumley, J, C. Cattell, R. Lysak, and J. Dombeck, Studies of ion solitary waves using simulations including hydrogen and oxygen beams, *J. Geophys. Res.*, 106, A4, 6007-6015, 2001.

De Lory G. T., et al. FAST Observations of Electron Distributions Within AKR Source Regions, *Geophys. Res. Lett.* Vol. 25, 12, 2069-2072, 1998.

Dombeck, J., e al., Observed trends in auroral zone ion mode solitary wave structure characteristics using data from Polar, *J. Geophys. Res.*, 106, A9, 19013-19021, 2001.

Eliasson, B. and Shukla, P., The dynamics of electron and ion holes, *Nonlin. Proc. Geophys.*, 12, 269 - 289, 2005.

Ergun R. E., et al., FAST Satellite Wave Observations in the AKR Source Region, *Geophys. Res. Lett.*, Vol. 25, 12, 2061-2064, 1998.

Ergun, R. E., et al., Electron-Cyclotron Maser Driven by Charge-Particle Acceleration From Magnetic Field-Aligned Electric Fields, *Astrophys. J.*, vol. 538, 456-466, 2000.

Farrell, W., Fine structure of the auroral kilometric radiation: A Fermi acceleration process? *Radio Sci.*, Vol. 30, 4, 961-973, 1995.

Farrell, W. et al., The radio search for extrasolar planets with LOFAR, *Plan. Sp. Sci.*, Vol. 52, 1469-1478, 2004.

Frank, C., T. Klinger, A. Piel, and H. Schamel, Dynamics of periodic ion holes in a forced beam-plasma experiment, *Phys. Plasmas*, 8,10, 4271-4274, 2001.

Grabbe, C., Theory of Fine Structure of Auroral Kilometric Radiation, *Geophys. Res. Lett.*, Vol. 9, Nr. 2, 155-158, 1982.

Green J. L. and Gallagher, D. L., The Detailed Intensity Distribution of the AKR Emission Cone, *J. Geophys. Res.*, Vol. 90, A10, 9641-9649, 1985.

Gurnett, D. et al., Initial Results form the ISEE-1 and 2 Plasma Wave Investigations, *Space Sci. Rev.*, Vol. 23, 103, 1979.

Gurnett, D. and R. Anderson, The Kilometric Radio Emission Spectrum: Relationship to Auroral Acceleration Processes, *Physics of Auroral Arc Formation*, Geophysical Monograph Series, Vol. 25. Ed. S.-I. Akasofu and J.R. Kan. Washington DC: American Geophysical Union, 341-350, 1981.

Gurnett, D, R. Huff, and D. Kirchner, The wide-band plasma wave investigation, Space Sci. Rev., 79, 195-208, 1997.

Hanasz, J., et al., Wideband bursts of auroral kilometric radiation and their association with UV auroral bulges, *J. Geophys. Res.*, vol. 106, A3, 3859-3872, 2001.

Kellett, B., R. Bingham, R. Cairns, and V. Tsikoudi, Can Late-type stars be explained by a dipoles magnetic trap? *M.N.R.A.S.*, 239, 102-108, 2002.

Kumamoto, A. and H. Oya, Asymmetry of Occurrence Frequency and Intensity of AKR between summer polar region and winter polar region, *Geophys. Res. Lett.* Vol. 25, 2369-2373, 1998.

Louarn, P., D. Le Quéau, and A. Roux, A new mechanism of stellar radiobursts: The fully energetic electron maser, *Astron. Astrophys.*, vol. 165, 211-217, 1986.

Louarn, P., A Roux, H. de Feraudy, D. Le Quéau, M. Andre, and L. Matson, Trapped electrons as a free energy source for the auroral kilometric radiation, *J. Geophys. Res.*, Vol. 95, 5983-5995, 1990.

McFadden J. P., et al., FAST Observations of Ion Solitary Waves, *J. Geophys. Res.*, Vol. 108, A4, 8018, 2003.

McKean, M. and R. Winglee, A model for the frequency fine structure of auroral kilometric radiation, *J. Geophys. Res.*, 96, A12, 21055-21070,1991.

Menietti D. et al., Discrete, Stimulated AKR Observed in the Galileo and DE 1 wideband Data, *J. Geophys. Res.* Vol. 101, A5, 10673-10680, 1996.

Menietti, D., Persoon, A., Pickett, J., and Gurnett, D., Statistical Studies of AKR fine Structure Striations Observed by Polar, *J. Geophys. Res.,* Vol. 105, A8, 18857-18866, 2000.

Morozova, E., M. Mogilevsky, J. Hanasz, and A. Rusanov, The Fine Structure of the AKR Electromagnetic Field as Measured by the Interball-2 Satellite, *J. Cosmic Res.,* Vol. 40, 4, 404-410, 2002.

Muschietti, L. et al., Modeling stretched solitary waves along magnetic field lines, *Nonlin. Proc. Geophys.*, 9, 101, 2002.

Omidi N. and Gurnett, D. A., Growth Rate Calculations of Auroral Kilometric Radiation Using the Relativistic Resonance Condition, *J. Geophys., Res.,* Vol. 87, A4, 2377, 1982.

Pottelette, R., R. Treumann, and M. Berthomier, Auroral Plasma Turbulence and the cause of the AKR fine structure, *J. Geophys. Res.* 106, A5, 8465-8476, 2001.

Pottelette R., Treumann, R. A., Berthomier, M., and Jaspers, J., Electrostatic Shock Properties Inferred from AKR Fine Structure, *Non. Proc. Geophys*, Vol. 10, 87-92, 2003.

Pottelette R. and Treumann R. A., Electron Holes in the Auroral Upward Current Region, *Geophys. Res. Lett.* , Vol. 32, L12104, 2005.

Pritchett P. L., Relativistic dispersion, the cyclotron maser instability, and auroral kilometric radiation, *J. Geophys. Res.*, Vol. 89, 8957-8970, 1984.

Pritchett P. L., et al., Free Energy Sources and Frequency Bandwidth for the Auroral Kilometric Radiation, *J. Geophys. Res.*, Vol. 104, A5, 10317-10326, 1999.

Pritchett P. L., R. Strangeway, R. Ergun, and C. Carlson., Generation and propagation of cyclotron maser emissions in the finite auroral kilometric radiation source cavity, *J. Geophys. Res.*, Vol. 107, A12, doi:10.1029/2002JA009403, 2002.

Roux A. et al., Auroral Kilometric Radiation Sources: In Situ and remote Observations From Viking, *J. Geophys. Res.*, Vol. 98, A7, 11657-11670, 1993.

Speirs, D., et al., A laboratory experiment to investigate auroral kilometric radiation emission mechanisms, *J. Plasma Phys..,* 71, Part 5, 665-674, 2005.

Strangeway, R. J. et al., FAST observations of VLF waves in the auroral zone: Evidence of very low plasma densities, *Geophys. Res. Lett.* 25, 12, 2065-2068, 1998.

Strangeway, R. J. et al., Accelerated Electrons as the Source of AKR, *Phys. Chem. Earth (C),* 26, 145-149, 2001.

Temerin, M. et al. , Observations of double layers and solitary waves in auroral plasmas, *Phys. Rev. Lett.,* 48, 1175, 1982.

Willes, A. and K. Wu, Electron-cyclotron maser emission from white dwarf pairs and white dwarf planetary systems, *M*.N.R.A.S., Vol. 348, 285-296, 2004.

Wu, C.S. and Lee, L. C., A Theory of the Terrestrial Kilometric Radiation, *Astrophys. J.*, Vol. 230, 621-626, 1979.

Yoon, P. and A. Weatherwax, A theory for AKR fine structure, *Geophys. Res. Lett.*, 25, 24, 4461-4464, 1998.

Zarka, P., Auroral Radio Emissions at the outer planets: Observations and theories, *J. Geophys. Res..*, 103, E9, 20,159-20194, 1998.

R. L. Mutel, Dept. Physics and Astronomy, University of Iowa, Iowa City IA 52242 (robert-mutel@uiowa.edu)

J. D. Menietti, Dept. Physics and Astronomy, University of Iowa, Iowa City IA 52242 (john-menietti@uiowa.edu)

I.W. Christopher, Dept. Physics and Astronomy, University of Iowa, Iowa City IA 52242 (ivar-christopher@uiowa.edu)

D. A. Gurnett, Dept. Physics and Astronomy, University of Iowa, Iowa City IA 52242 (donald-gurnett@uiowa.edu)

J.M. Cook, Dept. Physics and Astronomy, University of Iowa, Iowa City IA 52242 (justin-cook-2@uiowa.edu)